MICROWAVE SYNTHESIS OF BINARY GRAFTED *CASSIA FISTULA* GALACTOMANNAN FOR DYE REMOVAL

Preeti Kanchan[a], Huda Khanam[a], Arti Gautam[b], Deepak Kumar[c], Jyoti Pandey[a]

[a] *Department of Chemistry, B. B. Ambedkar University, Lucknow-226025 (U.P.), India*
[b] *Department of Microbiology, M. J. P. Rohilkhand University, Bareilly-243006 (U.P.), India*
[c] *Department of Chemistry, Constituent Government College, Richha, Baheri Bareilly M. J. P. Rohilkhand University, Bareilly-243006 (U.P.), India*

ABSTRACT

Cassia fistula gum (CFG) was modified through a microwave-assisted grafting method using acrylic acid (AA) and acrylamide (AM) to prepare CFG-g-(AA-co-AM). In addition, a crosslinked form CFG-cl-(AA-co-AM), was also synthesized using N,N′-methylenebisacrylamide (N-MBA) as crosslinking agent. Both the synthesized materials were evaluated for the removal of Congo Red dye from aqueous solutions. Structural characterization of the synthesized materials was carried out using FT-IR, XRD, TGA, and SEM-EDX techniques, confirming successful grafting and crosslinking. Batch adsorption studies were conducted to assess removal efficiency under different experimental conditions such as pH, dye concentration, temperature, contact time, and adsorbent dosage. Optimal adsorption performance was achieved with 30 mg adsorbent dose, an initial dye concentration of 100 ppm at 50 °C, pH 7, and 60 min contact time. Equilibrium data were analyzed using Langmuir and Freundlich isotherm models. The Langmuir model showed a superior fit with R^2 values of 0.9930 and 0.9933 for grafted and crosslinked samples, respectively, indicating monolayer adsorption. Kinetic studies were performed using various models, including first-order, second-order, pseudo-first-order, pseudo-second-order, intra-particle diffusion, and Elovich models. Among these, the Elovich model provided the best fit, suggesting that the adsorption process is predominantly controlled by chemisorption. Overall, the findings demonstrate that both grafted and crosslinked CFG-based materials are effective and low-cost adsorbents for the removal of dye from wastewater.

Key words: *Cassia fistula* galactomannan, grafting, crosslinking, Congo Red.

1. INTRODUCTION

The increasing degradation of global water resources due to anthropogenic contamination has become a serious environmental challenge (Khan et al., 2016). Industrial wastewater generally contains a complex mixture of pollutants, including heavy metals, synthetic dyes, pesticides, and pharmaceutical residues (Sousa et al., 2018). In addition, the persistence of these pollutants poses serious threats to human health and threatens aquatic biodiversity (Jadhav et al., 2019). Among these, synthetic dyes are the major contributors to water pollution, originating from various industries including plastics, paper and printing, textiles, and food processing. Among all, the textile industries are the major contributors to dye-contaminated wastewater, which is typically characterized by high chemical oxygen demand (COD), toxicity, and potential carcinogenicity (Rodrigues et al., 2023, Cao et al., 2016; Ji et al., 2016; Mallakpour et al., 2019; Modak et al., 2016; Bhatia et al., 2017). In most of the cases, industrial effluents are often discharged without adequate treatment, leading to the contamination of freshwater systems which reduces light penetration, thereby inhibiting photosynthesis and disturbing the ecological balance (Yan et al., 2013) and posing serious health risks (Kılıç, 2021). Synthetic organic dyes are particularly harmful because of their high toxicity and intense coloration, which significantly affect the optical and aesthetic quality of water bodies (Harfi et al., 2017). Even at trace levels, synthetic dyes adversely affect aquatic life causing severe toxic effects and may lead to serious health issues such as skin irritation and allergic reactions (Chen et al., 2019; Katheresan et al., 2018). Azo dyes account for approximately 60–70% of the total global dye production, and their complex aromatic frameworks confer high chemical stability, resistance to biodegradation, and intense coloration even at very low concentrations (Forgacs et al., 2004; Robinson et al., 2001). Among these, Congo red, an anionic diazo dye, is considered a significant environmental pollutant due to its high solubility in water, structural stability, and ability to produce toxic aromatic amines upon reductive cleavage (Liu et al., 2016; Saratale et al., 2011). Its persistence in aquatic environments reduces light penetration, suppresses photosynthetic processes, and exerts cytotoxic, mutagenic, and carcinogenic effects on living organisms (Hameed et al., 2008). As a result, the effective removal of Congo red from industrial effluents has become a major focus in wastewater treatment research (Koohi et al., 2021; Shayesteh et al., 2016). Conventional biological treatment methods are often inadequate for its removal because of its xenobiotic and recalcitrant nature, thereby necessitating the development of advanced and efficient treatment approaches. With the continuous growth of the textile industry, the elimination of Congo red and related azo dyes remains a critical environmental challenge. Therefore, the development of efficient and sustainable treatment strategies is essential

to control dye pollution (Zhou et al., 2019). Recently, polysaccharides and natural plant-based gums, including chitosan, alginate, xanthan gum, guar gum, tragacanth, acacia and gellan gum, have been extensively tailored through chemical modification for environmental remediation, driven by the need for sustainable and biodegradable alternatives to conventional synthetic materials (Vega-Hernández et al., 2021). A plant-based polysaccharide, *Cassia fistula* galactomannan (CFG), bears several hydroxyl groups that enable various chemical modifications. However, the unmodified CFG shows low affinity toward dye (Kanchan et al., 2026). Chemical modification through graft copolymerization is considered an effective approach for modifying polymer properties, enabling the development of materials with improved mechanical, thermal, and physicochemical characteristics (Kolya et al., 2014; Pal et al., 2021). This technique also enhances compatibility between different polymer systems. In the light of the above, a superabsorbent has been developed by modifying *Cassia fistula* polysaccharide through microwave-assisted grafting and cross-linking of acrylic acid and acrylamide using N,N′-methylenebisacrylamide (N-MBA) as cross-linking agent. The structural, morphological, and thermal properties of the synthesized material were analyzed using FTIR, SEM, XRD, and TGA techniques. The prepared grafted and cross-linked galactomannan was further evaluated for the adsorption of Congo Red dye from aqueous solutions. The effects of important parameters, including pH, contact time, adsorbent dosages, and temperature, were systematically investigated. The dye removal efficiency was determined using UV–Vis spectrophotometric analysis at 465 nm.

NEED OF THE STUDY

1. Research into the microwave-assisted synthesis of binary grafted galactomannans is essential for environmental sustainability in the waste water treatment.
2. By integrating microwave irradiation which optimizes synthesis efficiency with binary grafting to increase functional group density.
3. These materials are exclusively designed to target and eliminate hazardous dyes from industrial wastewater streams with high precision and speed.
4. The beauty of microwave method is that, this method does not require any inert atmospheric condition unlike the case of conventional method of synthesis.
5. The crosslinking and grafting of natural biopolymers with synthetic monomers (e.g., acrlylic acid and acrylamide etc.) is of great interest in the development of new materials due to the improved properties such as better process ability and biodegradability.

2. EXPERIMENTAL SECTION

2.1 Materials

Cassia fistula gum (CFG) was extracted from dry seeds collected from Babasaheb Bhimrao Ambedkar University. Acrylamide, acrylic acid, hydroquinone, N,N′-methylenebisacrylamide (N-MBA) and Congo Red dye were purchased from local supplier and used without further purification.

2.2 Characterization of CFG-cl-(AA-co-Am) and CFG-g-(AA-co-Am)

The vibrational characteristics of the grafted copolymers, CFG-g-(AA-co-Am) and CFG-cl-(AA-co-Am), were analyzed using Perkin Elmer Two FT-IR spectrophotometer. The measurements were carried out using the KBr pellet method, and spectra were recorded in the wavenumber range of 400–4000 cm^{-1} with a resolution of 2 cm^{-1}. The surface morphology and topographical features of the grafted materials were examined using scanning electron microscopy (SEM; JEOL JSM-6490LV). The crystalline nature of the samples was further investigated by X-ray diffraction (XRD) using a Bruker D8 Advance diffractometer equipped with Cu Kα radiation, within a 2θ range of 10–50°. The thermal stability and decomposition behavior of the grafted copolymers were evaluated by thermogravimetric analysis (TGA) using a PerkinElmer TGA 4000 instrument.

2.3 Dye adsorption study

Adsorption experiments were conducted to evaluate the performance of CFG-cl-(AA-co-Am) and CFG-g-(AA-co-Am) hydrogels under different experimental conditions. The effects of key parameters, including adsorbent dosage, initial solution pH, temperature, and contact time, were systematically investigated. The pH of the dye solution was adjusted using dilute HCl or NaOH as required. Congo Red, a commonly used anionic dye, was selected as the model pollutant for the adsorption studies. In a typical experiment, 30 mg of binary grafted/crosslinked hydrogel was added to 10 mL of a 100 ppm dye solution and maintained at 50 °C for 1 h. After adsorption, the remaining dye concentration in the solution was measured using a UV–Vis spectrophotometer at the maximum absorption wavelength (λmax = 465 nm), following the method reported by Lin et al. (2012). The amount of dye adsorbed by the hydrogel was calculated using a standard mass balance equation.

$$\text{Dye adsorption}(q) = \frac{C_o - C_e}{W} \times V \qquad (1)$$

Where,

C_o is the initial concentration of dye, C_e is the final concentration of dye, V is volume, W is the weight of the CFG-cl-(AA-co-Am) or CFG-g-(AA-co-Am).

3. RESULTS AND DISCUSSION

3.1 Synthesis of CFG-cl-(AA-co-AM)

The CFG-cl-(AA-co-Am) hydrogel was synthesized by dissolving 1.0 g of CFG gum in 100 mL of deionized water in an Erlenmeyer flask under constant stirring. Acrylic acid (AA) and acrylamide (Am) were then added to the aqueous solution in the required proportions. The reaction mixture was exposed to microwave irradiation at 1200 W for 90 s. Subsequently, the cross-linking agent, N,N′-methylenebisacrylamide (MBA), was added dropwise using a syringe to promote network formation (Kumar et al., (2018). The polymerization process was carried out under continuous stirring at 50 °C. To terminate the reaction, 0.5 mL of saturated hydroquinone solution was added as a free-radical inhibitor (Li et al., 2015). The resulting cross-linked hydrogel was then precipitated in ethanol and dried in an oven at 50 °C. The degree of Crosslinking of CFG was calculated by:

$$\% \text{ Crosslinking} = \frac{\text{wt. of crosslinked polymer}}{\text{wt. of pure polymer}} \times 100 \qquad (2)$$

3.2 Synthesis of CFG-g-(AA-co-AM)

Initially, 1.0 g of *Cassia fistula* gum was dissolved in 100 mL of double-distilled water under constant magnetic stirring. Acrylamide (Am) and acrylic acid (AA) were then added to the solution, and the mixture was stirred for 30 min to ensure uniform dispersion and molecular homogeneity. The reaction mixture was subsequently exposed to microwave irradiation at 1200 W (80% power) for 120 s to initiate the grafting process. A saturated hydroquinone solution was added as a radical scavenger to control the reaction. The obtained product was precipitated in ethanol, washed with acetone to remove residual impurities, and dried at 50 °C (Kumar et al., (2018). Percentage of grafting was evaluated by equation (3):

$$\% \text{ Grafting} = \frac{\text{wt. of grafted gum} - \text{wt. of pure gum}}{\text{wt. of pure gum}} \qquad (3)$$

4. Characterization

4.1 FTIR (Fourier Transmission Infrared Spectroscopy)

The FTIR spectrum of native *Cassia fistula* gum (CFG) exhibited several characteristic vibrational bands (Figure 1). A broad and intense absorption band at around 3400 cm^{-1} is attributed to O–H stretching vibrations of hydroxyl groups present in the polysaccharide backbone. The peak observed at 2927 cm^{-1} corresponds to C–H stretching vibrations, while the band at 1650 cm^{-1} is associated with pyranose ring vibrations. The region between 1650 and 813 cm^{-1} represents the fingerprint region, confirming the typical carbohydrate structure of the gum. Additionally, the bands at 1417 cm^{-1} and 1025 cm^{-1} are assigned to C–H bending and O–H bending vibrations, respectively. The grafted copolymer CFG-g-(Am-co-AA) (Figure 1) showed new characteristic peaks, indicating successful modification. A distinct peak at 1728 cm^{-1} is assigned to C=O stretching of carboxylic acid groups from acrylic acid. The band at 1413 cm^{-1} corresponds to N–H bending (amide II), while the peak at 1155 cm^{-1} confirms the presence of amide groups derived from acrylamide. The appearance of these new functional group signals, along with a reduction in the intensity of the original CFG peaks, confirms the successful grafting of acrylic acid and acrylamide onto the CFG backbone. The FTIR spectrum of the cross-linked copolymer, CFG-cl-(AA-co-Am), is also presented in Figure 1. The broad peak in the native gum at around 3400 cm^{-1} become sharp indicating the formation of intermolecular hydrogen bonding between hydroxyl groups of native gum and carboxyl groups of acrylic acid and amide groups of acrylamide, in the grafting process. The absorption band at 2955 cm^{-1} is attributed to C–H stretching vibrations. Furthermore, the peak at 1610 cm^{-1} (amide I, C=O stretching) and the band at 1411 cm^{-1} (C–N stretching) provide clear evidence of successful cross-linking. The appearance of additional peaks in the range of 719–668 cm^{-1}, corresponding to N–H out-of-plane bending vibrations, further supports the incorporation of acrylamide units into the cross-linked network.

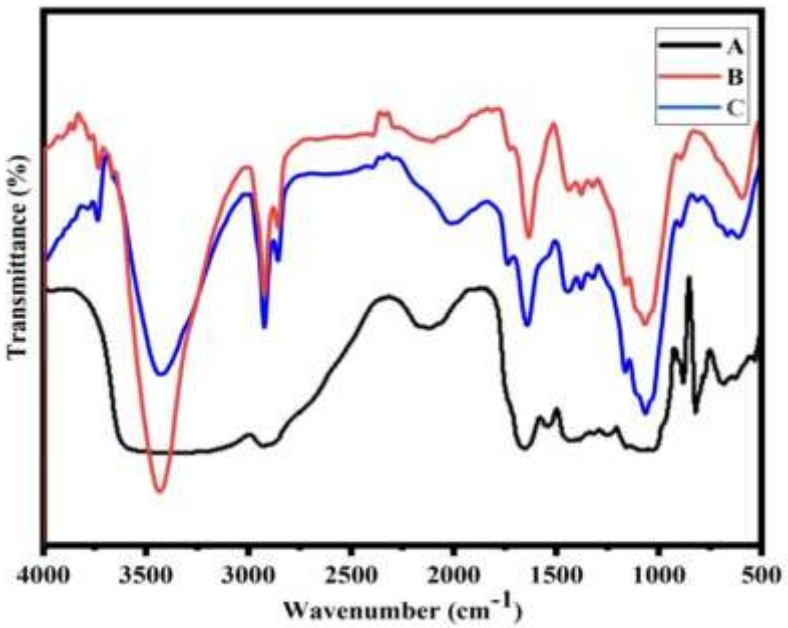

Fig 1. The FT-IR spectra of (A) *Cassia fistula* gum, (B) CFG-g- (Am-co-AA), (C) CFG-cl-(AA-co-Am)

4.2 SEM (Scanning electron microscopy)

The surface morphologies of native Cassia fistula gum (CFG), the grafted copolymer CFG-g-(Am-co-AA), and the cross-linked copolymer CFG-cl-(AA-co-Am) were examined using SEM and EDX analysis (Figure 2& 3). The SEM micrographs of native CFG revealed a heterogeneous surface with irregular structures. After microwave-assisted grafting with acrylamide and acrylic acid, the surface morphology became more heterogeneous compared to the native gum, indicating structural modification of the polymer matrix. The corresponding EDX spectra (Figure 3) further supported this modification by confirming the presence of elements associated with nitrogen-containing and carboxylic functional groups. In contrast, the cross-linked material, CFG-cl-(AA-co-Am), exhibited a comparatively rough and highly heterogeneous surface, suggesting the formation of a more complex and interconnected network structure.

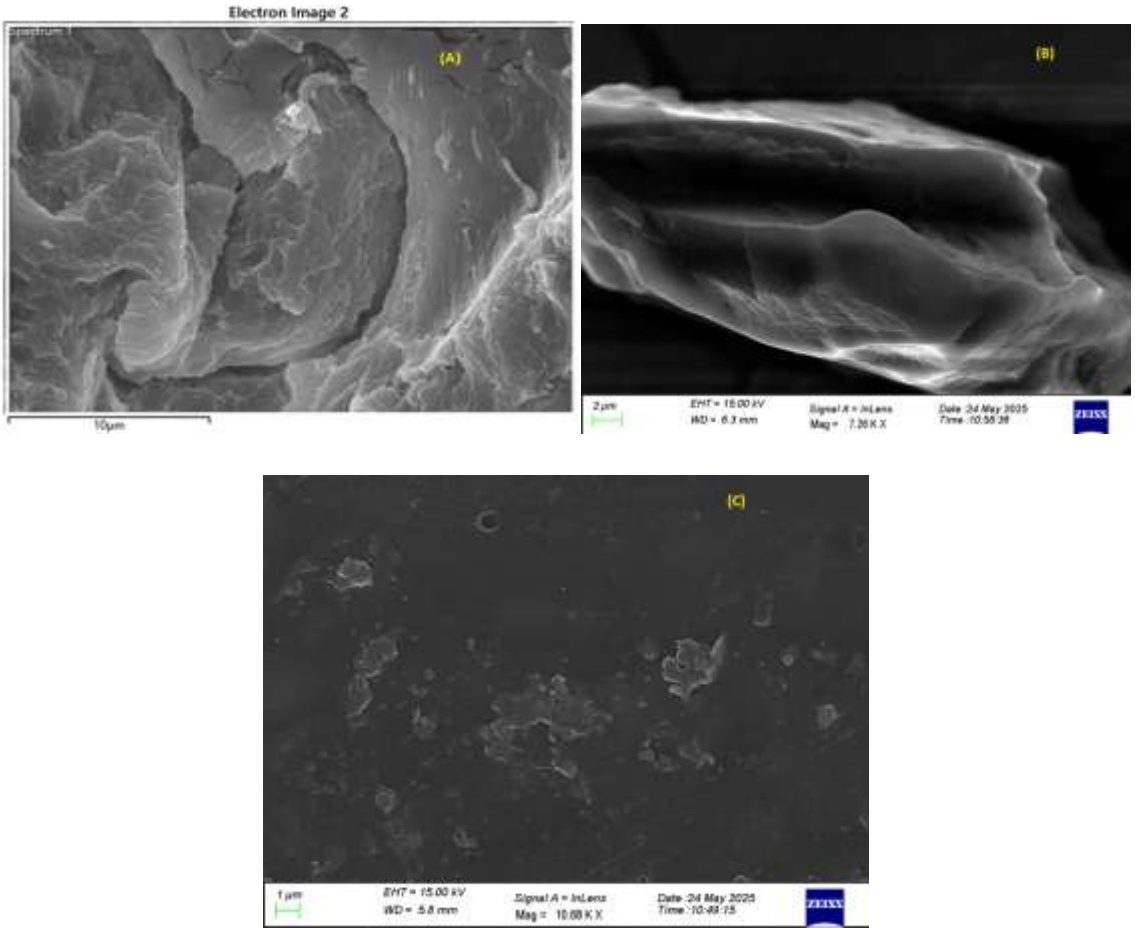

Figure 2. (A) SEM images of CFG gum, (B) CFG-cl-(AA-co-AM) and (C) CFG-g-(AA-co-AM).

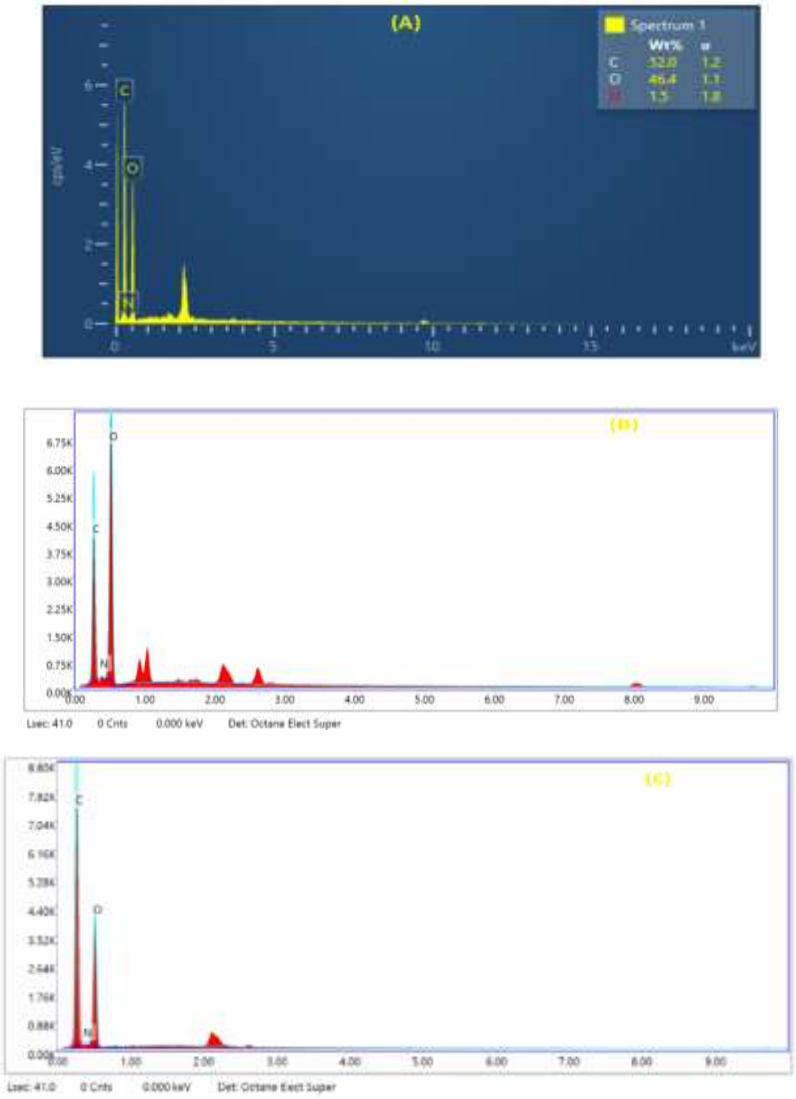

Figure 3. (A) EDX spectrum of CFG gum, (B) CFG-cl-(AA-co-AM) and (C) CFG-g-(AA-co-AM).

4.3 XRD (X-ray diffraction)

The XRD patterns of native *Cassia fistula* gum (CFG), the grafted copolymer CFG-g-(Am-co-AA), and the cross-linked network CFG-cl-(AA-co-Am) are presented in Figure 4. The XRD spectrum of native CFG exhibits a broad peak at $2\theta \approx 17°$, indicating amorphous nature of the gum. After microwave-assisted grafting/cross-linking of acrylamide and acrylic acid on to the CFG backbone, the diffraction peak of native CFG gum disappeared, indicating a reduction in structural order due to the successful incorporation of monomers onto the CFG backbone. This clearly indicates that the material retains an amorphous nature even after grafting/cross-linking. Such a disordered structure is beneficial for adsorption applications, as it facilitates solvent penetration and enhances swelling behaviour.

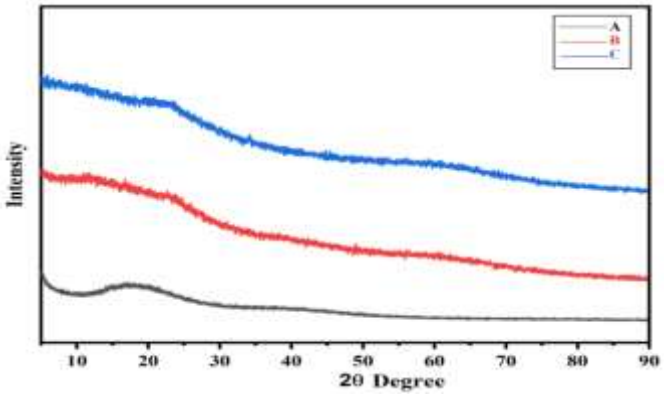

Figure 4. The XRD spectra of (A) Cassia fistula gum, (B) CFG-cl-(AA-co-Am) and (C) CFG-g- (Am-co-AA).

5. Dye removal study

5.1 Effect of temperature

The effect of temperature on the adsorption of Congo Red dye was investigated over a range of 20–60 °C, and the results are presented in Figure 5 & 6. An increase in dye removal efficiency was observed with increasing temperature from 20 °C to 30 °C. The grafted as well as cross-linked binary grafted CFG showed a slight improvement in adsorption efficiency, with the removal percentage increasing up to ~99% over the studied temperature range.

5.2 Effect of time

The contact time between the adsorbent, CFG-g-(Am-co-AA), and the Congo Red dye, is an important parameter influencing the adsorption kinetics. The variation in dye removal with time is presented in Figure 5 & 6. It was observed that adsorption occurred rapidly during the initial stage after the addition of the grafted hydrogel to the dye solution. For the grafted CFG-g-(Am-co-AA), a removal efficiency of approximately 98% was achieved within 50 min, after which the system approached equilibrium. Similarly, the cross-linked CFG-cl-(AA-co-Am) exhibited comparable adsorption performance, reaching a removal efficiency of about 98% within the same time period (60 min).

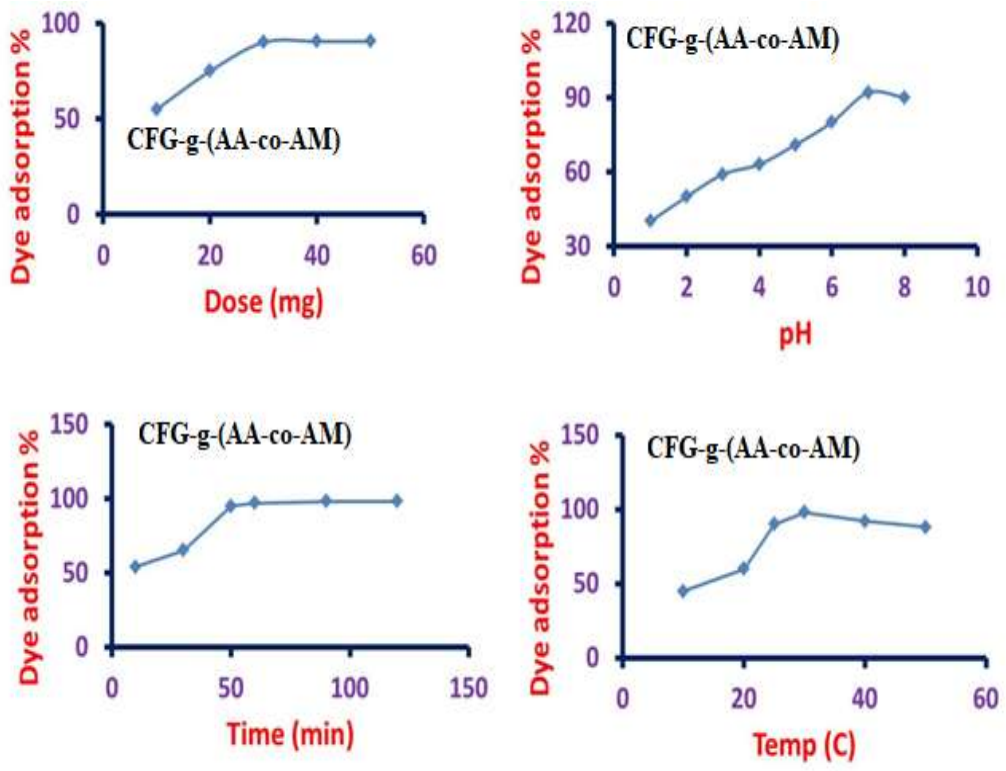

Figure 5. Dye removal percentage of grafted [CFG-g-(AA-co-AM)] gum with respect to dose, pH, time and temperature.

5.3 Effect of pH

pH is an important parameter in the adsorption process, as it affects both the surface charge of the adsorbent and the adsoption of the dye molecules. The effect of pH was investigated using a 100 ppm Congo Red (CR) solution and an adsorbent dosage of 30 mg over a pH range of 3–10, as shown in Figure 5 & 6. A gradual decrease in adsorption efficiency was observed with increasing pH from acidic to alkaline conditions. The maximum removal efficiency (~98%) was achieved at near-neutral pH (around pH 7) for both the grafted and cross-linked CFG samples, after which the adsorption efficiency declined. This behaviour can be attributed to the deprotonation of functional groups on the adsorbent surface at higher pH values, resulting in the development of negative surface charge. Consequently, electrostatic repulsion occurs between the negatively charged adsorbent surface and the anionic Congo Red molecules, leading to a reduction in adsorption capacity.

5.4 Effect of adsorbent dose

The effect of adsorbent dosage on the adsorption of Congo Red (CR) was investigated by varying the dosage from 10 to 60 mg in 10 mL of a 100 ppm dye solution. After a contact time of 50 min, the suspensions were centrifuged to separate the supernatant, which was then analyzed using UV–Vis spectroscopy. As shown in Figure 5 & 6, the dye removal efficiency of CFG-g-(AA-co-Am) increased with increasing adsorbent dosage and reached an optimum range of 96–98% at 30 mg. This improvement can be attributed to the greater availability of active adsorption sites and an increased surface area. However, further increase in adsorbent

dosage beyond 30 mg resulted in a plateau, where the removal efficiency remained nearly constant. Therefore, 30 mg was considered the optimum dosage for a 100 ppm dye solution. The cross-linked material, CFG-cl-(AA-co-Am), also exhibited similar behaviour, achieving a maximum removal efficiency of approximately 98% with 30 mg dose.

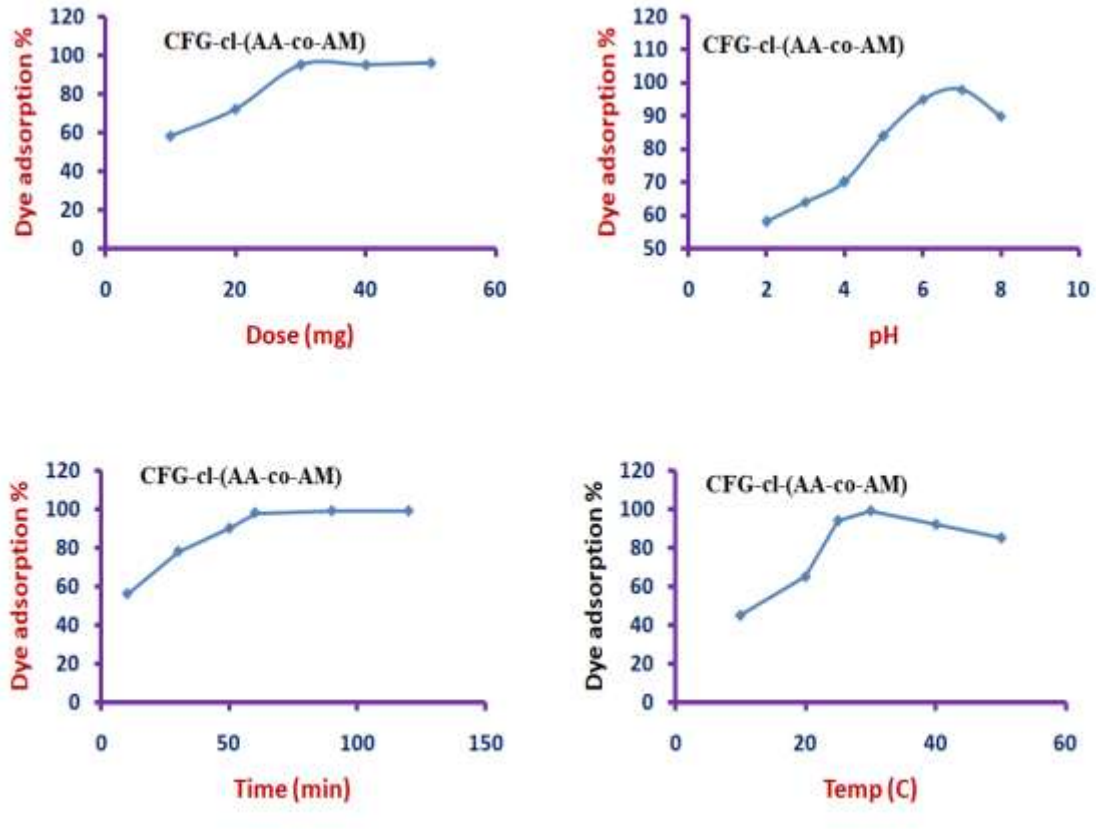

Figure 6. Dye removal percentage of grafted [CFG-cl-(AA-co-AM)] gum with respect to dose, pH, time and temperature.

5.5 Adsorption isotherms and models

5.5.1 Langmuir adsorption isotherm

The Langmuir adsorption isotherm is widely used to describe monolayer adsorption onto a surface containing a finite number of energetically identical and equivalent active sites. This model assumes that once an adsorbate molecule occupies a specific site, no further adsorption can occur at that site, indicating the formation of a molecular monolayer.

For the determination of the isotherm constants, the Langmuir model is commonly expressed in its linearized form, as given in Equation (4).

$$\frac{C_e}{Q_e} = \frac{K_L}{Q_m} + \frac{C_e}{Q_m} \quad (4)$$

where

C_e = Equilibrium concentration

Q_e = Amount adsorbed at equilibrium

K_L = Langmuir constant related to adsorption affinity

Q_m = maximum adsorption capacity

$$R_L = \frac{1}{(1 + K_L C_o)} \quad (5)$$

Where, C_o is initial concentration (mg/L) and adsorption is considered favorable when the $R_L$value lies between 0 and 1.

5.5.2 Freundlich adsorption isotherm

The Freundlich isotherm characterizes the heterogeneous surface energy through multilayer adsorption and presents the linear form as shown in the equation (6).

$$lnq_e = lnK_F + \frac{1}{n} lnC_e \quad (6)$$

where, K_f = adsorbent adsorption capacity

The Freundlich parameters (K_f), correlation constant (R^2), and rate constant were determined using the Freundlich isotherm.

Both the Langmuir and Freundlich models were applied to evaluate the adsorption isotherm of CFG-g-(AA-co-Am), and CFG-cl-(AA-co-Am) hydrogels.

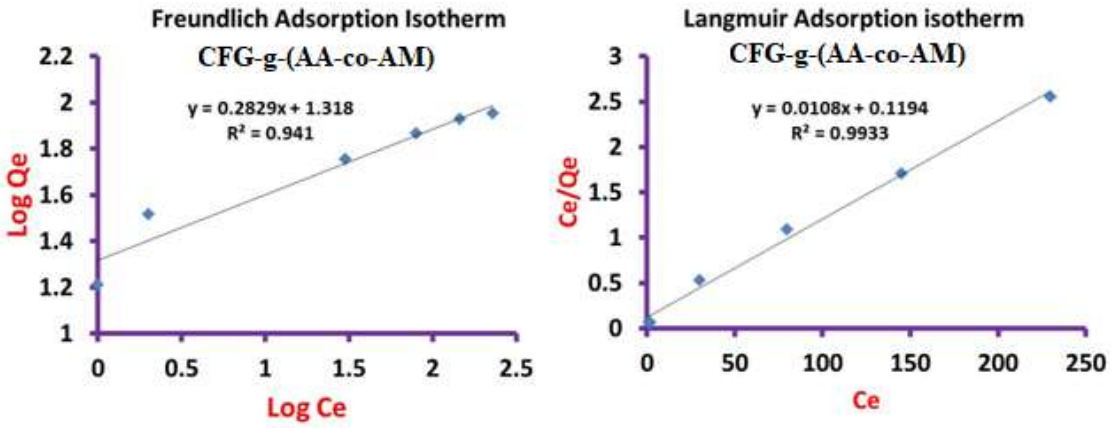

Figure 7. Freundlich and Langmuir adsorption isotherm graph of CFG-g-(AA-co-AM).

For the grafted sample, CFG-g-(AA-co-Am), the adsorption isotherm analysis using both Freundlich and Langmuir models is presented in Figure 7. The Freundlich model (log C_e) showed a correlation coefficient (R^2) of 0.9410. The Langmuir model (C_e) exhibited an excellent fit with a higher correlation coefficient (R^2 = 0.9933), indicating monolayer adsorption on a relatively homogeneous surface. The maximum adsorption capacity (Qm) obtained from the Langmuir model was 92.59 mg g^{-1}, indicating a high affinity of the adsorbent for Congo Red dye and the calculated values of R_L and K_L were 0.5841 and 0.0904 mL mg^{-1}, respectively, confirming favorable adsorption behavior (Table 2).

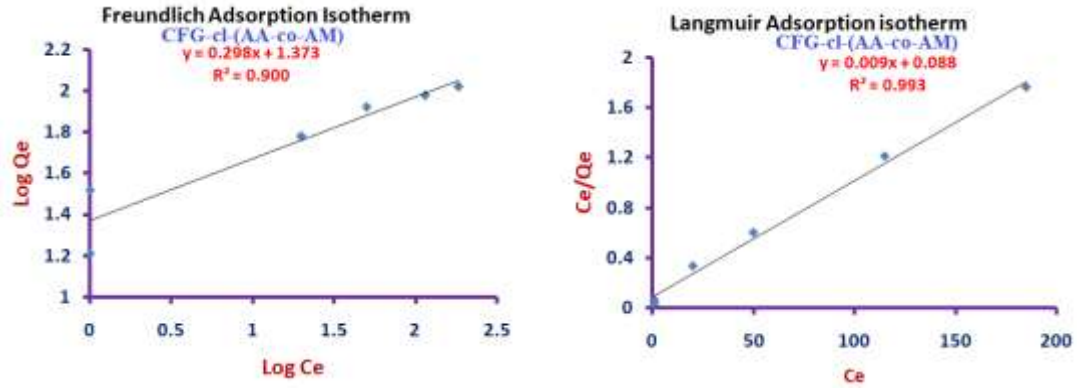

Figure 8. Freundlich and Langmuir adsorption isotherm graph of CFG-cl-(AA-co-AM).

In the case of the cross-linked sample, CFG-cl-(AA-co-Am), the adsorption isotherm analysis using both Freundlich and Langmuir models is presented in Figure 8. The Freundlich model (log C_e) showed a correlation coefficient (R^2) of 0.9000, and the slope value (1/n=0.298) corresponds to n≈3.355, suggesting favorable adsorption, while the intercept gives a Freundlich constant (K_f) of approximately 23.60 mg g^{-1}. The Langmuir model (C_e) exhibited an excellent fit with a higher correlation coefficient (R^2 = 0.9930), indicating monolayer adsorption on a relatively homogeneous surface. The maximum adsorption capacity (Q_{max}) was calculated to be approximately 111.11 mg g^{-1}, and the Langmuir constant (K_L) was found to be ~0.102 L mg^{-1}. Overall, the better fit of the Langmuir model suggests that monolayer adsorption is the dominant mechanism for Congo Red removal by the cross-linked hydrogel as presented in Table 2.

Table 2. Adsorption isotherm parameters Freundlich and Langmuir model from CFG-g-(AA-co-AM) and CFG-cl-(AA-co-AM).

S. No	Parameter	CFG-g-(AA-co-AM)	CFG-cl-(AA-co-AM)
[A] Freundlich Isotherm			
1	K_f (antilog of intercept)	20.80	23.60
2	n (1/slope)	3.534	3.355
3	R^2	0.9410	0.9000
[B] Langmuir Isotherm			
1	Q_m (1/slope) (mg/g)	92.59	111.11
2	K_L (Slope/intercept) (L/mg)	0.0904	0.10227
3	$R_L = 1 / (1 + K_L \times C_0)$	0.0996	0.0892
4	R^2	0.9933	0.9930

5.6 Kinetic Studies

The kinetic study regarding the adsorption of dye onto CFG-g-(AA-co-AM) and CFG-cl-(AA-co-AM) was conducted by applying the pseudo-second, pseudo-first, second, first order, intra-particle diffusion and Elovich models. The results are illustrated in Figure 9 & 10.

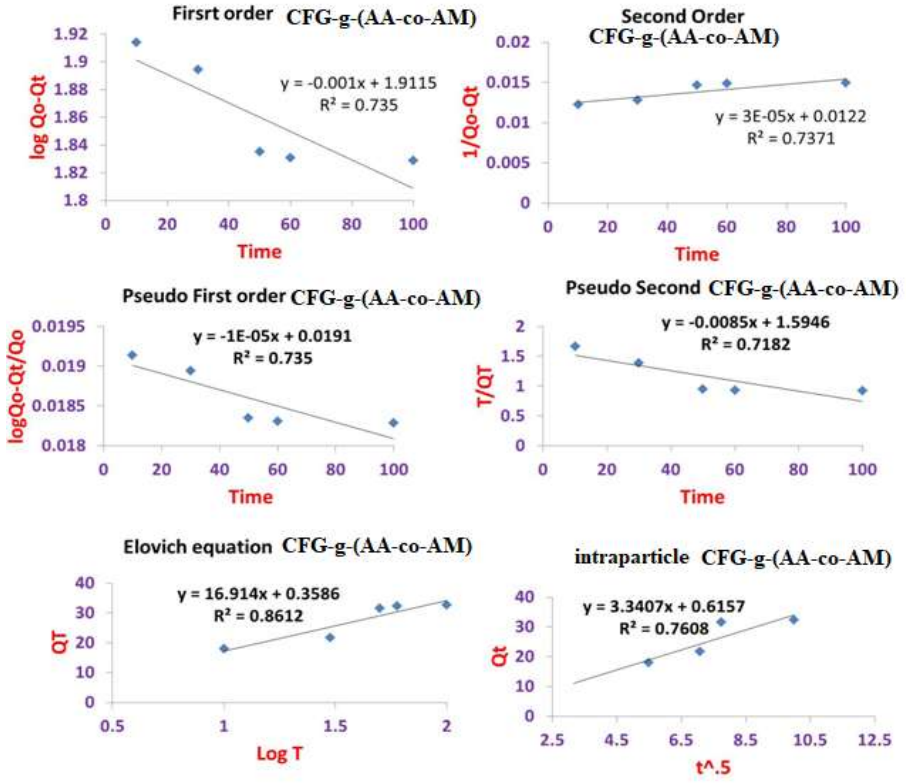

Figure 9. Kinetic models of CFG-g-(AA-co-AM).

5.6.1 First-Order Kinetic Equation

The linear representation of the first-order kinetics equation is expressed as Eq. (7).

$$\ln \frac{Qo}{Qt} = k_1 t \qquad (7)$$

Where, Q_o (mgL^{-1}) and Q_t (mgL^{-1}) represent the concentrations of dye at the initial time (time zero) and at a specified time 't', respectively. K_1 (min^{-1}) denotes the first order rate constant.

Rate constant, and the regression coefficient R^2 derived from the linear plot of $\ln(Q_o/Q_t)$ against t as shown in Figure 9 and 10. In CFG-g-(AA-co-AM), R^2 value is 0.7350 and for CFG-cl-(AA-co-AM), R^2 value is 0.7852 as presented in Table 3.

5.6.2 Second Order Kinetic Equation

The linear equation of second-order kinetics equation is given in Equation (8):

$$\frac{1}{(Q_o - Q_t)} = k_2 t \quad (8)$$

Where, k_2 [Lmg^{-1} min^{-1}] is the second order rate constant and calculated from the slope of linear plot of $\frac{1}{(Q_o - Q_t)}$ against t as shown in Figure 9 and 10. The values of the constants are given in Table 3.

5.6.3 Pseudo-First-Order Kinetic Equation

The linear form pseudo-first-order equation is given in Equation. (9)

$$\log \frac{(Q_o - Q_t)}{Q_o} = \log Q_o - \frac{k_1 t}{2.303} \quad (9)$$

where, Q_0, Q_t, and k_1 represent the concentrations of dye at the initial time (time zero) and at a specified time 't', and the rate constant, respectively. All the parameters were derived from this equation are presented in Table 3.

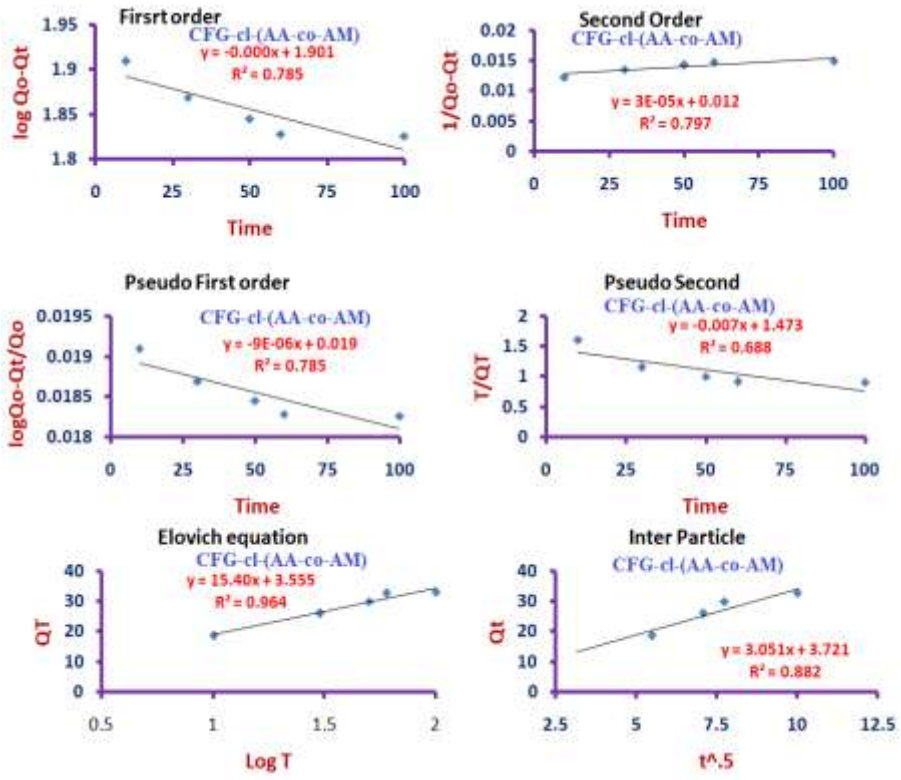

Figure 10. Kinetic models of CFG-cl-(AA-co-AM).

5.6.4 Pseudo-Second Order Kinetics Equation

The pseudo-second-order kinetic rate was analyzed using Eq. (10)

$$\frac{t}{Q_t} = \frac{t}{k_2 Q_e^2} + \frac{t}{Qe} \quad (10)$$

Where, k_2 denotes the rate constant. The graph for Eq. (10) are shown in Figure 9 and 10, and the values of all parameters are provided in the Table 3. The R^2 value is 0.7182 from CFG-g-(AA-co-AM) and R^2 value is 0.6888 from CFG-cl-(AA-co-AM) in Table 3.

5.6.5 Intraparticle Diffusion

Eq. (11) represents the intraparticle diffusion kinetic equation.

$$Q_t = k_{id}\, t^{1/2} + C \quad (11)$$

Where, k_{id} represents the rate constant (mg/g $min^{-1/2}$) and C denotes the intraparticle diffusion constant (mg/g). Figure 9 and 10, illustrates the intraparticle diffusion kinetic curve for dye adsorption, and the computed values of the intraparticle diffusion parameters are provided in Table 3.

5.6.6 Elovich Model

The Elovich equation is expressed in Equation. (12).

$$Q_t = \frac{1}{\beta}\ln(\alpha\beta) + \frac{1}{\beta}\ln(t) \quad (12)$$

Where, Q_t signifies the amount of dye adsorbed at time t, and α (g/mg) and β (mg/g^{-1} min^{-1}) are the Elovich constants. The values of α and β were determined using the linear plot of Q_t vs ln(t) as shown in Figure 9 and 10.

Table 3. The kinetic models data from grafted CFG-g-(AA-co-AM) and cross-linked CFG-cl-(AA-co-AM).

S.No	Model	Parameter	CFG-cl-(AA-co-AM)	CFG-g-(AA-co-AM)
1.	**Pseudo-First-Order**	k_1 (min^{-1})	-9×10^{-6}	-1×10^{-5}
		Intercept	0.019	0.0191
		R^2	0.785	0.735
2.	**First-Order**	slope	-0.00	-1×10^{-3}
		intercept	1.901	1.9115
		R^2	0.785	0.735
3.	**Pseudo-Second-Order**	slope	−0.007	-0.0085
		intercept	1.473	1.5946
		R^2	0.688	0.7182
4.	**Second-Order**	slope	3×10^{-5}	3×10^{-5}
		intercept	0.012	0.0122
		R^2	0.797	0.7371
5.	**Elovich Model**	α (mg/g/min)	15.4	16.914
		R^2	0.964	0.8612
6.	**Intraparticle Diffusion**	K_{id} (mg/g·min$^{1/2}$)	3.051	3.3407
		C	3.721	0.6157
		R^2	0.882	0.7608

CONCLUSIONS

In this study, grafted (CFG-g-(AA-co-Am)) and cross-linked (CFG-cl-(AA-co-Am)) *Cassia fistula* gum-based hydrogels were successfully synthesized using a microwave-assisted method. Characterization studies confirmed the successful incorporation of acrylic acid and acrylamide into the polymer backbone. The synthesized materials exhibited excellent adsorption performance toward Congo Red dye, with maximum removal efficiency observed at near-neutral pH. Adsorption kinetics followed the Elovich model, suggesting chemisorption on heterogeneous surfaces. Isotherm analysis revealed that the adsorption process is best described by the Langmuir model, indicating monolayer adsorption behaviour. The cross-linked hydrogel showed slightly higher adsorption capacity due to its improved structural network. Overall, the developed materials demonstrate strong potential as efficient and eco-friendly adsorbents for wastewater treatment applications.

Acknowledgements

P. K. thanks CSIR for JRF fellowship, H.K thanks UP-CST for Research Assistantship, A.G and D.K are also thankful to M J P Rohilkhand University, Bareilly–243006 (U.P.), India.

REFERENCES

1) Bhatia, D.; Sharma, N. R.; Singh, J.; Kanwar, R. S. (2017). Biological methods for textile dye removal from wastewater: A review. *Critical Reviews in Environmental Science and Technology*, 47, 1836–1876.

2) Cao, X.; Luo, J.; Woodley, J. M.; Wan, Y. (2016). Bioinspired multifunctional membrane for aquatic micropollutant removal. ACS Applied Materials & Interfaces, 8, 30511–30522.

3) Chen, W.; Mo, J.; Du, X.; Zhang, Z.; Zhang, W. (2019). Biomimetic dynamic membrane for aquatic dye removal. Water Research, 151, 243–251.

4) El Harfi, S.; El Harfi, A. (2017). Classification, properties and applications of textile dyes: a review. Applied Journal of Environmental Engineering Science, 3(3), 311–320.
5) Forgacs, E.; Cserháti, T.; Oros, G. (2004). Removal of synthetic dyes from wastewaters: a review. Environ. Int., 30, 953–971.
6) Hameed, B. H.; Daud, F. B. M. (2008). Adsorption studies of basic dye on activated carbon derived from agricultural waste: Hevea brasiliensis seed coat. Chem. Eng. J., 139, 48–55.

7) Jadhav, S. A.; Garud, H. B.; Patil, A. H.; Patil, G. D.; Patil, C. R.; Dongale, T. D.; Patil, P. S. (2019). Recent advancements in silica nanoparticle-based technologies for dye removal from water. Colloid and Interface Science Communications, 30, 100181.

8) Ji, C.; Hou, J.; Chen, V. (2016). Cross-linked carbon nanotube-based biocatalytic membranes for micropollutant degradation: performance, stability and regeneration. Journal of Membrane Science, 520, 869–880.

9) Kanchan, P.; Gautam, A.; Kumar, D.; Pandey, J. (2026). Exploration of *Cassia fistula* galactomannan for dye removal applications. Goya Journal (Accepted manuscript)

10) Katheresan, V.; Kansedo, J.; Lau, S. Y. (2018). Efficiency of various recent wastewater dye removal methods: a review. Journal of Environmental Chemical Engineering, 6, 4676–4697.

11) Khan, S. A.; Khan, S. B.; Kamal, T.; Yasir, M.; Asiri, A. M. (2016). Antibacterial nanocomposites based on chitosan-Co-MCM as selective and efficient adsorbents for organic dyes. International Journal of Biological Macromolecules, 91, 744–751.

12) Kılıç, Z. (2021). Water pollution: causes, negative effects, and prevention methods. ˙ Istanb. Sabahattin Zaim Üniv. Fen Bilim. Enst. Derg. 3 (2), 129–132.

13) Kolya, H.; Das, S.; Tripathy, T. (2014). Synthesis of starch-g-poly(N-methylacrylamide-co-acrylic acid) and its application for the removal of mercury(II) from aqueous solution by adsorption. European Polymer Journal, 58, 1–10.

14) Koohi, P. Rahbar-kelishami, A. Shayesteh, H. (2021). Efficient removal of Congo red dye using Fe3O4/NiO nanocomposite: synthesis and characterization. Environ. Technol. Innov., 23, 101559.

15) Kumar, D.; Pandey, J.; Kumar, P. (2018). Microwave-assisted synthesis of binary grafted psyllium and its utility in anticancer formulation. Carbohydrate Polymers, 179, 408–414.

16) Kumar, R.; Chandra, R.; Dubey, R. (2016). Synthesis and characterization of cross-linked polymers of acrylic acid and psyllium mucilage. Journal of Technology and Advanced Science Research, 2, 185–189.

17) Li, Y.; Wang, M.; Huang, H.; Yan, H.; Yang, H.; Xiao, S.; Li, A. (2015). Preparation of chitosan-graft-polyacrylamide magnetic composite microspheres for enhanced selective removal of mercury ions from water. Journal of Colloid and Interface Science, 455, 261–270.

18) Lin, J.; Huang, A.; Dufresne, A. (2012). Preparation, properties and applications of polysaccharide nanocrystals in advanced functional nanomaterials: a review. Nanoscale, 4(11), 3274–3294.
19) Liu, Z.; Zhang, F.; Liu, T.; Peng, N.; Gai, C. (2016). Removal of azo dye by a highly graphitized and heteroatom doped carbon derived from fish waste: adsorption equilibrium and kinetics. J. Environ. Manag., 182, 446–454.

20) Mallakpour, S.; Rashidimoghadam, S. (2019). Carbon nanotubes for dye removal. In: Composite Nanoadsorbents, 211–243.

21) Modak, J. B.; Bhowal, A.; Datta, S. (2016). Extraction of dye from aqueous solution in a rotating packed bed. Journal of Hazardous Materials, 304, 337–342.

22) Pal, R. R.; Kumar, D.; Raj, V.; Rajpal, V.; Maurya, P.; Singh, S.; Tiwari, N. (2021). Synthesis of pH-sensitive cross-linked guar gum-g-poly(acrylic acid-co-acrylonitrile) for drug delivery of thymoquinone against inflammation. International Journal of Biological Macromolecules, 182, 1218–1228.
23) Robinson, T.; McMullan, G.; Marchant, R.; Nigam, P. (2001). Remediation of dyes in textile effluent: a critical review on current treatment technologies with a proposed alternative. Bioresour. Technol., 77, 247–255.

24) Rodrigues, A. F.; da Silva, A. F.; da Silva, F. L.; dos Santos, K. M.; de Oliveira, M. P.; Nobre, M. M.; dos Santos, J. C. (2023). A scientometric analysis of research progress and trends in the design of laccase biocatalysts for the decolorization of synthetic dyes. Process. Biochem. 126, 272–291.

25) Saratale, R. G.; Saratale, G. D.; Chang, J. S.; Govindwar, S. P. (2011). Bacterial decolorization and degradation of azo dyes: a review. J. Taiwan Inst. Chem. Eng., 42, 138–157.

26) Shayesteh, H.; Rahbar-Kelishami, A.; Norouzbeigi, R. (2016). Evaluation of natural and cationic surfactant modified pumice for Congo red removal in batch mode: kinetic, equilibrium, and thermodynamic studies. J. Mol. Liq., 221, 1–11.

27) Sousa, J. C.; Ribeiro, A. R.; Barbosa, M. O.; Pereira, M. F. R.; Silva, A. M. (2018). A review on environmental monitoring of water organic pollutants identified by EU guidelines. Journal of Hazardous Materials, 344, 146–162.

28) Vega-Hernández, M. A.; Cano-Díaz, G. S.; Vivaldo-Lima, E.; Rosas-Aburto, A.; Hernández-Luna, M. G.; Martinez, A.; Palacios-Alquisira, J.; Mohammadi, Y.; Penlidis, A. (2021). A review on the synthesis, characterization and modeling of polymer grafting. Processes, 9, 375.

29) Vishnu, D.; Dhandapani, B.; Authilingam, S.; Sivakumar, V. (2022). A comprehensive review of effective adsorbents used for the removal of dyes from wastewater. Current Analytical Chemistry, 18(3), 255–268.

30) Yan, H.; Li, H.; Yang, H.; Li, A.; Cheng, R. (2013). Removal of various cationic dyes from aqueous solutions using a biodegradable magnetic composite microsphere. Chemical Engineering Journal, 223, 402–411.

31) Zhou, Y.; Lu, J.; Zhou, Y.; Liu, Y. (2019). Recent advances in dye removal using novel adsorbents: a review. Environmental Pollution, 252, 352–365.